046

Dynamic Stall on a Fully Equipped Helicopter Model

K. Kindler[1,†], K. Mulleners[1], and M. Raffel[1]

[1]Institute of Aerodynamic and Flow Technology, DLR Göttingen, Germany
[†]*Current address*: Max Planck Institute for Marine Microbiology, Bremen, Germany

Abstract

Three-dimensional dynamic stall was observed on the rotor of a fully equipped sub-scale helicopter model in a wind tunnel. Results of stereoscopic particle image velocimetry measurements on the retreating blade clearly revealed the large-scale dynamic stall vortex at 50% and 60% blade radius. The location of the axes of small-scale shear layer vortices that constitute the dynamic stall vortex were extracted. Based on the spatial distribution of these small-scale vortices, the characteristic large-scale structure was found to be unexpectedly compact. Along with an apparent spanwise flexion of the dynamic stall vortex, these results suggested the rotational motion to have a stabilising effect on the formation and convection of this predominant feature. The velocity field information which is now available is also believed to be valuable for validation of recent computational fluid dynamics investigations of three-dimensional dynamic stall.

1 Introduction

Dynamic stall (DS) on an airfoil comprises a series of complex aerodynamic phenomena in response to an unsteady change of the angle of attack [2, 8, 9]. It is accompanied by a lift overshoot and delayed massive flow separation with respect to static stall. The salient feature of the unsteadily separating flow is the formation and convection of a large-scale coherent structure referred to as the dynamic stall vortex. The most prominent example can be observed on the retreating blades of an helicopter rotor in forward flight.

Hitherto, experimental investigations have been limited to two-dimensional DS on oscillating airfoils [10, 8, 1, 14] and DS on finite wings of small aspect ratio [20, 3]. Computational fluid dynamics (CFD) investigations on the other hand, have been constrained by challenges in turbulence modelling in unsteady flows and limited computational performance. Only recently, CFD studies of three-dimensional DS on large aspect-ratio planforms, i.e. generic helicopter blades have become available (cf. [19]). Previous two-dimensional DS studies have lead to a deeper understanding of the complicated flow phenomena involved, but they have also clearly demonstrated the need to include and examine the inherent three-dimensionality of the rotor operating environment. Finite wing and rotational effects as well as the influence of blade lag motion have to be considered for a comprehensive understanding of DS on helicopter rotors.

Three-dimensional DS on finite wings is essentially characterised by the interaction of the tip vortices and the DS vortex which results in the emergence of a localised arched separation region in the mid-span section of the wing [6, 17, 11]. Due to the downwash induced by the wing tip vortices the effective angle of attack is increased in the mid-span region leading to a faster growth of the DS vortex here. The latter consists of a combination of the rolled-up shear layer and the remnants of several vortices generated by a shear layer instability [12, 18]. The spanwise variation of the growth rate causes the DS vortex to arch away from the wings surface, yielding a bucking shape resembling a capital omega (cf. [6]). The outboard segments are pinned to the surface and are weaker than the dominant central part of the vortex, which can be presumed quasi-two-dimensional. In the outboard region the three-dimensionality – and thus the complexity – of the flow field increases due to the influence of the wing tip vortex and the accompanied tip arching of the predominantly tranverse dynamic stall vortex.

When passing over to the rotor environment, the concurrence of yaw angles and rotation leads to a variation in the effective angles of incidence along the span. The influence of the yaw angle and the rotation of a large aspect ratio blade on DS were

investigated numerically by *Spentzos* [19]. To the authors' knowledge, this is the only available (numerical) study of the subject and it reveals a asymmetric arched DS vortex which is shifted towards the outboard side of the blade.

Further advancement of DS prediction and modelling with regard to helicopter rotors requires further numerical studies on three-dimensional DS in a rotating frame of reference as well as additional experimental investigations to validate and complement the numerical results. In the framework of the EU-project GoAHEAD (**G**eneration **o**f **A**dvanced **H**elicopter **E**xperimental **A**erodynamic **D**atabase for CFD code validation) a fully equipped model of a generic medium size transport helicopter was investigated in the Large Low-speed Facility (LLF) of the German-Dutch Wind Tunnels (DNW) [13, 16]. In particular, phase-locked, high-resolution, three-component velocity field data of the dynamic stall vortex were obtained directly within the rotating system. Thereby, a first quantitative insight into DS on helicopter rotors has become available and will be presented and discussed here. Furthermore, based on the gained insights and the experimental difficulties encountered, further avenues of inquiry will be suggested.

2 Experimental Methods

The helicopter model consisted of a scaled NH90 fuselage including all control surfaces, main, and tail rotor. A 40 % Mach-scaled ONERA 7AD main rotor was used with parabolic tips and included a rotor hub. The blade radius was $R = 2.1\,\mathrm{m}$ with $c = 0.14\,\mathrm{m}$ reference chord length, yielding an aspect ratio $Æ = 15$. The main rotor had a build-in inclination angle of $-5°$ with respect to the fuselage and the blades featured $\tau = -8.3°/R$ linear twist. The model was positioned in the centre of the $8 \times 6\,\mathrm{m}^2$ closed test section of the wind tunnel.

Since the test conditions for DS were considered high-risk for the integrity of the model, stall onset was approached by varying the trim parameters at a free-stream and rotor tip Mach number of $Ma_\infty = 0.259$ and $Ma_{MR} = 0.617$ respectively, and $\alpha = -3.95°$ angle of attack. The angular velocity of the main rotor was $\Omega = 101.1\,\mathrm{rad/s}$ corresponding to an advance ratio $\mu = U_\infty/(\Omega R) = 0.42$ with

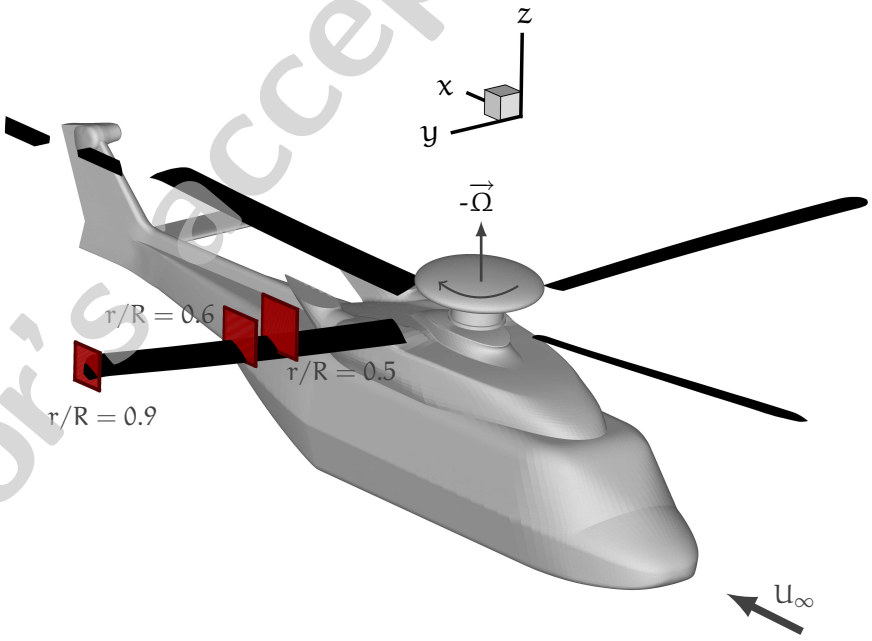

Figure 1: Schematic representation of the experimental configuration and the positions of the measurement planes on the retreating blade at $\psi_v = 272.3°$.

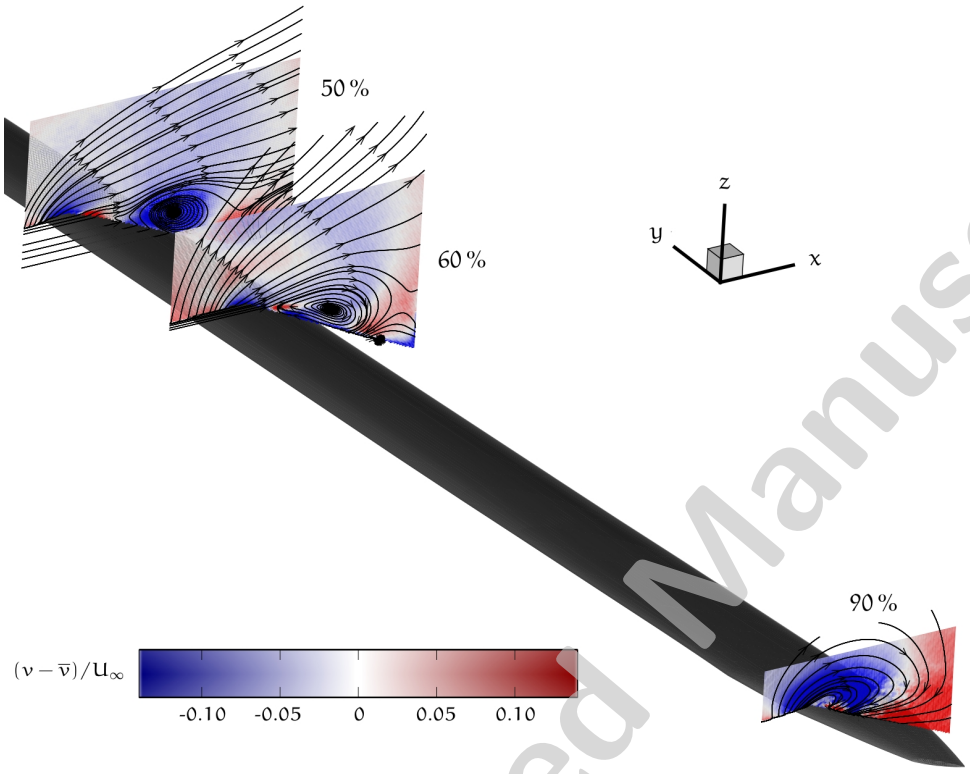

Figure 2: The footprint of dynamic stall in the three measurement planes at r/R =0.5, 0.6, and 0.9, at $\psi = 272.3°$ in azimuth; the scaled, phase averaged out-of-plane velocity component v is colour-coded while the in-plane components u, w are depicted as stream lines.

U_∞ = 88.3 m/s. When the power, vibration, control, and actuator force limits were reached, a pitch link force spike in the range of $\psi = 180°$ to 270° was encountered indicating stall inception[1].

Stereoscopic PIV data was acquired at three radial positions, r/R =0.5, 0.6, and 0.9 (figure 1) on the retreating blade at $\psi = 270°$ to 276° using standard procedures [15]. Illumination was provided by a double-cavity Nd:YAG laser with a pulse energy of 2×280 mJ fanned out into a light sheet and directed into the test section from the ceiling of the wind tunnel. In order to reduce light reflections on the upper surface of the blade, the light sheet access was located far downstream from the model in order to achieve an approximately tangential impingement on the surface of the blade. Due to the limited optical access, the observation regions on the blade were inclined by 22°, 21°, and 3° at r/R =0.5, 0.6, and 0.9 with respect to chord. Series of $N = 100$ images were acquired through lateral windows in the wind tunnel wall using a pair of high-resolution pco.2000 cameras with 200 mm lenses. Image acquisition was pulse-triggered by the main rotor with the cameras operating at a multiple of the rotor frequency. The size of the fields of view were 0.23 m × 0.22 m to 0.164 m × 0.164 m. The corresponding spatial resolutions varied between 1.4 mm and 1 mm.

3 Results and Discussion

3.1 Phase averaged flow fields

At a free-stream and rotor Mach number of Ma_∞ = 0.259 and Ma_{MR} = 0.617 respectively, a large-scale coherent DS vortex can be clearly identified at r/R = 0.5 and 0.6 whereas at the most outboard position r/R = 0.9 a fully separated flow is observed, which is moreover strongly three-dimensional (cf. figure 2). In this region the blade tip vortex interacts with the outboard segment of

[1]Conventionally $\psi = 0°$ denotes the rear, i.e. downstream, position of the blade.

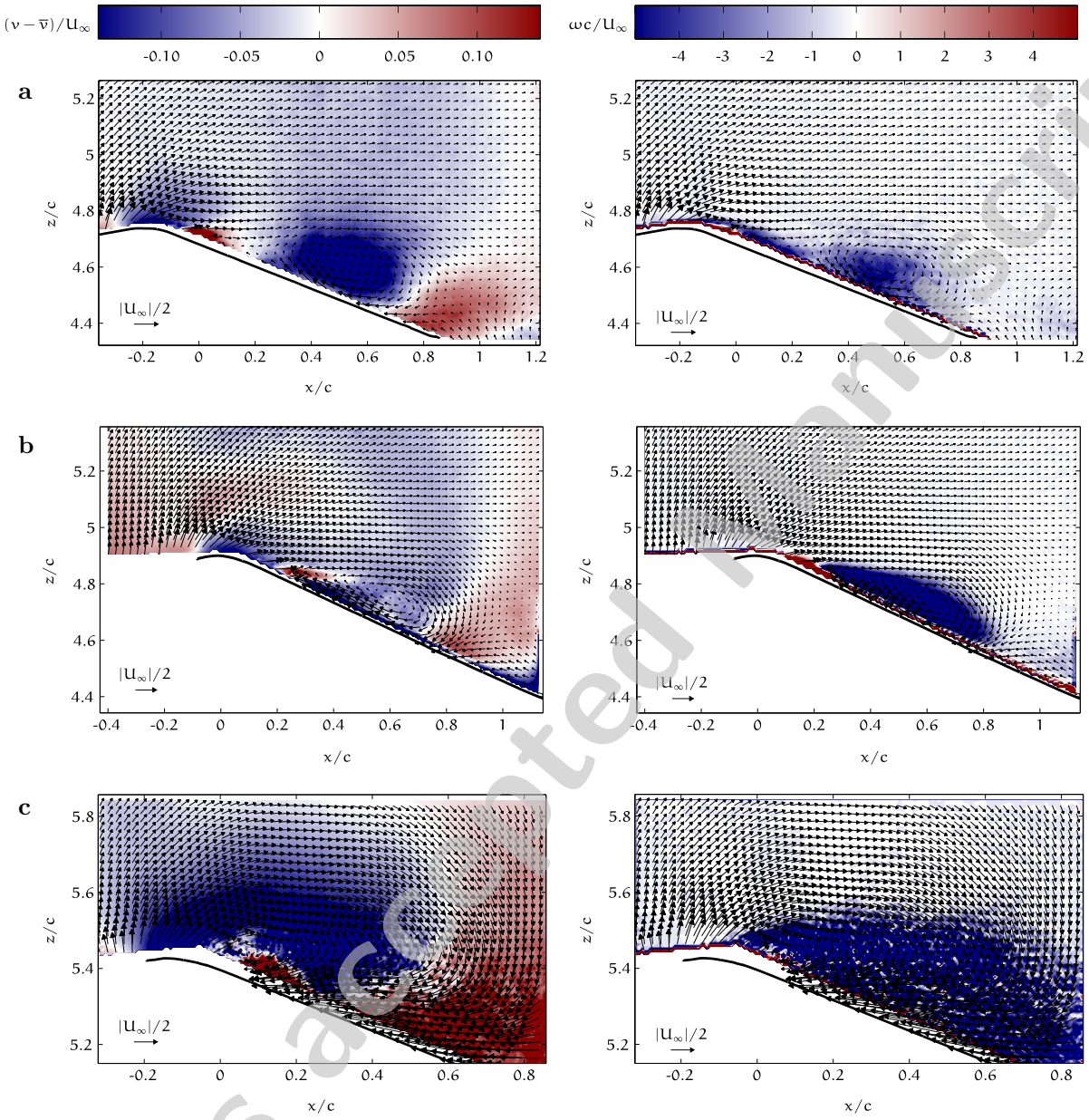

Figure 3: The scaled, phase averaged velocity (left) and the in-plane vorticity component (right) at $\psi = 272.3°$ and $r/R = 0.5$ (**a**), 0.6 (**b**), and 0.9 (**c**).

the DS vortex.

More detailed views of the phase averaged velocity fields[2] along with the in-plane vorticity fields are depicted in figure 3. It can be readily observed that the chord-wise position of the DS vortex is virtually unchanged between $r/R = 0.5$ and 0.6. In this spatial region the DS vortex thus appears to be stretched virtually parallel to the leading edge, which is in good agreement with recent CFD results by *Spentzos* [19]. However, this large-scale structure is noticeably flatter at $r/R = 0.6$ than at mid-span while the associated region of concentrated in-plane vorticity ω_y is distinctly enlarged. Furthermore, the radial or out-of-plane velocity component

[2]The free stream velocity U_∞ has been subtracted in all vector fields. The out-of-plane component is normalised as $(v-\overline{v})/U_\infty$ with $\overline{v}$ taken far from the blade surface.

at $r/R = 0.5$ is strongly negative, i.e. directed outboard, in a concentrated region covered by the DS vortex (see figure 3a). The area of strong outboard swirling flow is flanked at both sides by patches of inboard directed flow. The latter is still valid at $r/R = 0.6$ (figure 3b). However, the strength of the outboard directed velocity component is attenuated and the extent of the region covered by it is reduced.

3.2 Sub-structures of the dynamic stall vortex

Although the DS vortex appears as a single compact vortical structure in the image sequence of figure 3, it is essentially formed by the roll up of the shear layer that emerged at the interface between the separated flow near the airfoil's surface and the free stream flow. Hence, the DS vortex is composed of a multitude of small-scale vortices generated by a primary instability of this shear layer. To study the constitution and compactness, as well as the cycle to cycle stability of the large-scale DS vortex, the individual small-scale vortical structures were identified and localised by means of a Galilean invariant, Eulerian vortex axis identification procedure. The position of the centre of vortical structures in the ensemble of velocity fields was determined utilising the following scalar function introduced by Graftieaux et al. [5]:

$$\Gamma_2(P) = \frac{1}{N} \sum_S \frac{[PM \times (U_M - \tilde{U}_P)]\, \hat{e}_y}{\| PM \| \cdot \| U_M - \tilde{U}_P \|}, \qquad (1)$$

where N is the number of points in the two dimensional neighbourhood S of any given point P in the x, z plane, M lies in S, $\hat{e}_y$ is the unit vector in y direction, and $\tilde{U}_P$ is the local convection velocity around P. The local extrema of Γ_2 are associated with the location of vortex centres[3].

Unlike alternative vortex identification criteria, such as vorticity concentration, λ_2, etc., the Γ_2 function does not require the evaluation of velocity field gradients and is therefore less susceptible to experimental noise. For a comprehensive review of the diversity and robustness of gradient-based vortex detection methods it should be referred to [7, 4].

The spatial distribution of all individual small-scale shear layer vortices extracted from the ensemble of instantaneous velocity fields at $r/R = 0.5$ and 0.6 is depicted in figure 4 and overlayed by the phase average in-plane velocity field. Additionally, histograms represent the vertical and streamwise distributions separately. Noticeably, especially for readers familiar with two-dimensional DS experiments, is the very localised distribution of the small-scale structures. The conclusions here are twofold. First, the strong confinement refers to a spatially very compact DS vortex which remains in close proximity to the airfoil's surface. This is somewhat different from what is usually observed in two-dimensional measurements (cf. [12, 18]). Hence, the rotation of the blade and the associated span-wise velocity gradient seem to have a stabilising effect on the DS vortex, preventing it to fall apart. Second, the spreading of the vortex positions due to the cycle to cycle variations must be relatively small.

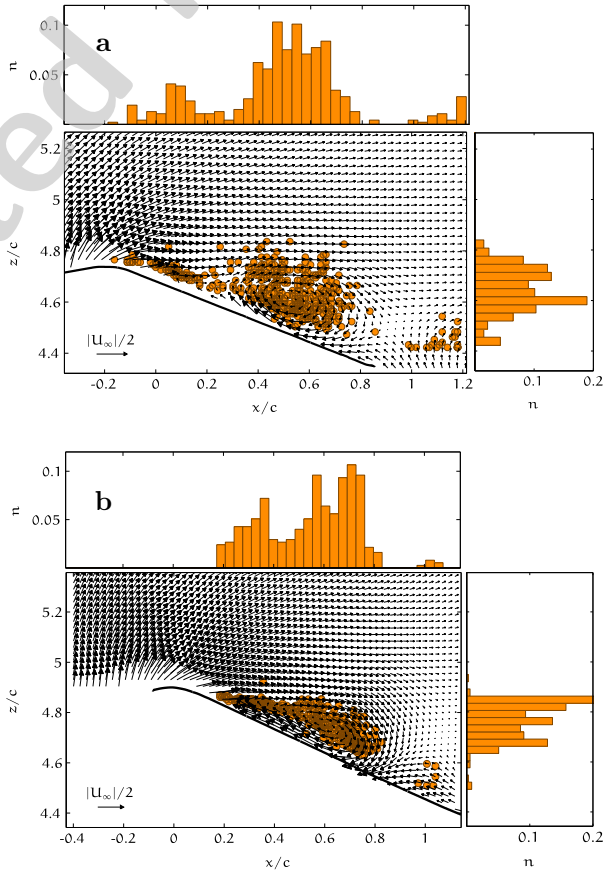

Figure 4: The in-plan velocity, the centre positions of sub-structures composing the DS vortex and the distribution of centre positions at $\psi = 272.3°$ for $r/R = 0.5$ (**a**), 0.6 (**b**).

[3]Note that Γ_2 is not to be confused with the circulation of a vortex.

4 Conclusions and Directions for Future Experiments

Dynamic stall was directly observed on the retreating blade of the rotor of a fully equipped subscale helicopter model during wind tunnel tests. The characteristic DS vortex was identified and appeared to be stretched almost parallel to the leading edge in the region covering the measurement planes at 50% and 60% blade radius. At $r/R = 0.9$ the blade tip vortex interacted with the outboard segment of the DS vortex yielding increased three-dimensionality and complexity of the flow field. Based on the identification and analysis of the individual small-scale shear layer vortices composing the DS vortex, the latter is found to be spatially concentrated. This is attributed to a combination of rotational and finite wing effects.

These first quantitative insights into the DS phenomenon on helicopter rotors are believed to be highly valuable for validation of computational fluid dynamics investigations. Nevertheless, extensive experimental efforts including the rotor operating environment are required in order to contribute to the fundamental understanding of three-dimensional DS on helicopters. In this context, the spanwise development and deformation of the DS vortex needs to be further analysed. In particular, information about the interaction of the end segment of the DS vortex with the reversed flow region and the blade tip vortex is of utmost interest. Additional investigations of the whole DS life cycle by means of high-fidelity PIV are highly desirable in order to model and predict the complex aerodynamic phenomena attributed to DS. For this purpose it is envisaged to build the image acquisition system into the rotor hub and to provide a rotating laser sheet from above the rotor axis. By doing so, the continuous observation of the velocity field and the development of the characteristic DS vortex as a function of azimuthal position will be possible.

Acknowledgements This work has been part of the European Commission funded project "Generation of Advanced Helicopter Experimental Aerodynamic Database for CFD code validation" (GoAhead). Valuable discussion and support by the project partners is greatfully acknowledged.

References

[1] L.W. Carr. Progress in analysis and prediction of dynamic stall. *J. Aircraft*, 25(1):6–17, 1988.

[2] L.W. Carr, K.W. McAlister, and W.J. McCroskey. Analysis of the development of dynamic stall based on oscillating airfoil experiments. TN D-8382, NASA, 1977.

[3] F. N. Coton and R. A. McD. Galbraith. An experimental study of dynamic stall on a finite wing. *Aeron. J.*, 103(1023):229, 1999.

[4] R. Cucitore, M. Quadrio, and A. Baron. On the effectivenss and limitations of local criteria for the identification of a vortex. *Eur. J. Mech. B. Fluids*, 18(2):261–282, 1999.

[5] L. Graftieaux, M. Michard, and N. Grosjean. Combining PIV, POD and vortex identification algorithms for the study of unstready turbulent swirling flows. *Meas. Sci. Technol.*, 12:1422–1429, 2001.

[6] M.B. Horner. Controlled three-dimensionality in unsteady separated flows about a sinusoidally oscillating flat plate. In *Proceedings of the* 28^{th} *Aerospace Science Meeting, Reno, Nevada, USA*, number AIAA Paper 90-0689, January 8–11 1990.

[7] J. Jeong and F. Hussain. On the identification of a vortex. *J. Fluid Mech.*, 285:69–94, 1995.

[8] K.W. McAlister, L.W. Carr, and W.J. McCroskey. Dynamic stall experiments on the NACA0012 airfoil. TP 1100, NASA, 1978.

[9] W.J. McCroskey. The phenomenon of dynamic stall. TM 81264, NASA, 1981.

[10] W.J. McCroskey and R.K. Fisher. Dynamic stall of airfoils and helicopter rotors. AGARD R 595, AGARD, 1972.

[11] S. Moir and F.N. Coton. An examination of the dynamic stalling of two wing planforms. Aero. Rept. 9526, Glasgow University, 1995.

[12] K. Mulleners and M. Raffel. A time-resolved dynamic stall investigation based on coherent structure analysis. In *15th International Symposium on Applications of Laser Techniques to Fluid Mechanics, Lisbon, Portugal, July 5–8*, 2010.

[13] K. Pahlke. The GoAHEAD project. In *Proceedings of the* 33^{rd} *European Rotorcraft Forum*, Kazan, Russia, September 11–13 2007.

[14] M. Raffel, J. Kompenhans, and P. Wernert. Investigation of the unsteady flow velocity field above an airfoil pitching deep dynamic stall conditions. *Exp. Fluids*, 19:103–111, 1995.

[15] M. Raffel, C. Willert, S. Wereley, and J. Kompenhans. *Particle Image Velocimetry, A practical guide*. Springer, 2004.

[16] M. Raffel, F. de Gregorio, W. Sheng, G. Gibertini, A. Seraudie, K. de Groot, and B.G. van der Wall. Generation of an advanced helicopter experimental aerodynamic database – The wind tunnel test of the EU-project GoAHEAD. In *Proceedings of the* 35^{th} *European Rotorcraft Forum*, Hamburg, Germany, September 22–25 2009.

[17] S.J. Schreck and H.E. Helin. Unsteady vortex dynamics and surface pressure topologies on a finite wing. *J. Aircraft*, 31(4):899–907, 1994.

[18] C. Shih, L. Lourenco, L. Van Dommelen, and A. Krothapalli. Unsteady flow past an airfoil pitching at constant rate. 30(5):1153–1161, May 1992.

[19] A. Spentzos, G. N. Barakos, K. J. Badcock, and B. E. Richards. Modelling three-dimensional dynamic stall of helicopter blades using computational fluid dynamics and neural networks. *Proc. IMechE Vol. 220 Part G; J. Aerospace Eng*, page 605, 2006.

[20] J. Szafruga and B.R. Ramaprian. LDA measurements in the three-dimensional flow over an oscillating wing. In *28th AIAA Fluid Dynamics Conference, Snowmass, CO, 29 June – 2 July*, 1997.